IEICE TRANS. COMMUN., VOL.E94–B, NO.8 AUGUST 2011

PAPER

2-Dimensional Accurate Imaging with UWB Radar Using Indoor Multipath Echoes for a Target in Shadow Regions

Shuhei FUJITA[†a)], ***Student Member***, **Takuya SAKAMOTO**[†], ***Member***, ***and*** **Toru SATO**[†], ***Fellow***

SUMMARY UWB (Ultra Wide-Band) pulse radar is promising for surveillance systems because it has an outstanding high range-resolution. To realize an accurate UWB radar imaging system, we propose a new approach that employs multipath echoes from a target in an indoor environment. Using multipath echoes, the proposed system can accurately estimate images, even for targets in a shadow region where the targets are out of sight of the antenna. We apply a simple interferometry technique using the multiple mirror image antennas generated by multipath propagation. We find that this simple method also produces many undesired false image points. To tackle this issue, we also propose an effective false image reduction algorithm to obtain a clear image. Numerical simulations verify that most of the false image points are removed and the target shape is accurately estimated.

key words: *UWB pulse radar, multipath scattering waves, shadow region imaging, interferometry, Time-Reversal imaging*

1. Introduction

Surveillance systems are indispensable for maintaining a safe society, and preventing crimes and terror attacks. Most of the current security systems use cameras due to their low-cost and high resolution capabilities. A system using radiowaves is another candidate for this purpose because it has the potential to avoid some of the substantial limitations of camera-based systems. It has been reported that radiowaves enable the detection of targets in hidden places where cameras cannot work. Existing communication infrastructure like WLAN stations has been employed for positioning purposes [1], [2]. Although these methods are capable of estimating target locations, the resolution is not good enough to estimate the shape of the target.

To obtain this information, UWB (Ultra Wide-Band) pulse radar is promising for surveillance imaging because of its high range resolution. To achieve high cross-range resolution, most of the conventional algorithms [3]–[5] including the SEABED method [6], [7] use array antennas. These costly and large-scale systems are not realistic for commercial surveillance systems. Another approach using the motion of targets [8] has been developed to obtain an image using only 3 antennas. Furthermore, a new approach, the TR (Time-Reversal) method [9], [10] using multipath echoes makes it possible to calculate an image using only a single antenna [11], [12]. Assuming a point-like target, this method numerically back-propagates the received signal in a known-shaped room to focus on an image at the target location. The method cannot estimate a target shape although it gives an accurate target location.

In this paper, we propose a new imaging method for UWB radar with only a single antenna that combines the ideas of the TR and the interferometry method [13] to accurately estimate a target shape in a multipath environment. This method also has a particular advantage over conventional camera-based systems because it enables the imaging of a target in an area that is out of sight. The proposed method picks up multipath echoes from the received signals to estimate the target shape. The procedure gives a correct target shape with many undesirable false images caused by the ambiguity of the propagation paths corresponding to multipath echoes in the received signals. To eliminate these false images, we also propose an effective false image reduction algorithm to obtain a clear image. First, we explain the procedure of the proposed imaging method, followed by some numerical simulation results to show the performance of the proposed method compared to conventional methods.

2. System Model

For simplicity, we deal with a 2-dimensional problem in this paper. It is assumed that a radar system is installed on a mechanical scanner in a room as in Fig. 1. We assume that the room is configured as a known polygonal shape. A target (a human) is located at an unknown position in the room. The room has a blind area blocked by walls. The areas where direct waves cannot be received from the antenna are called shadow regions in this paper. Figure 2 shows an example of the shadow region blocked by a wall in a room. The

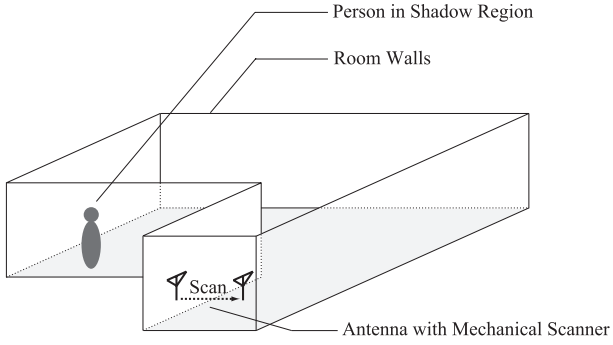

Fig. 1 Overview of surveillance system using UWB pulse radar.

Manuscript received June 9, 2010.
Manuscript revised February 14, 2011.

[†]The authors are with the Department of Communications and Computer Engineering, Graduate School of Informatics, Kyoto University, Kyoto-shi, 606-8501 Japan.
a) E-mail: fujita-syuhei@denden18.mbox.media.kyoto-u.ac.jp

DOI: 10.1587/transcom.E94.B.2366

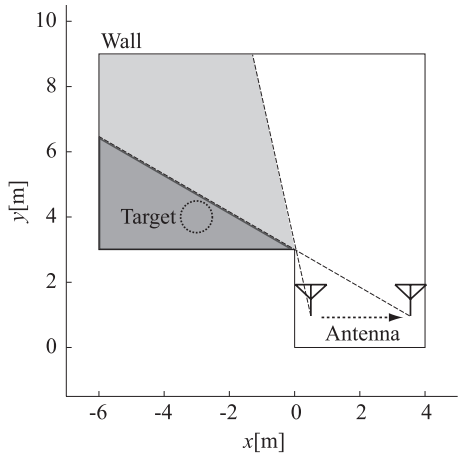

Fig. 2 System model A with a shadow region.

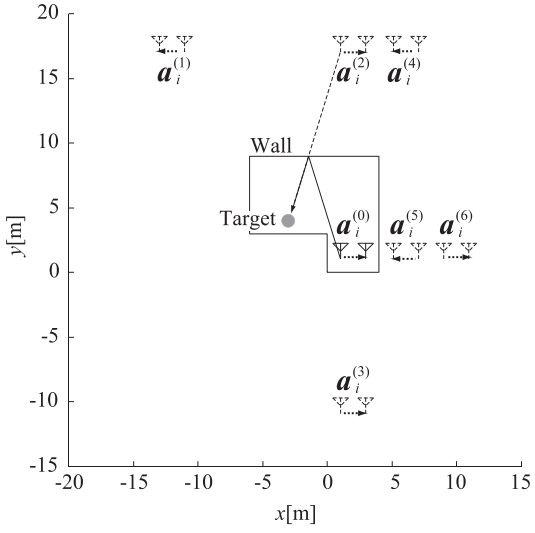

Fig. 3 Mirror image antennas for model A.

shadow region in the system is defined as the intersection of the shadow regions for all the antenna locations, which means that the shadow region is the area not visible from any location along the antenna-scanning line. The region painted the darkest gray in Fig. 2 represents the shadow region.

Figure 3 shows a model of the system, where an antenna and a target are located in an L-shaped room made of PEC (Perfect Electric Conductor). We define real space as the space where the target and the antenna are located. We express the real space with the parameters $\boldsymbol{r} = (x, y)$. The target is modeled as a simple-shaped PEC object in the shadow region. The reflection coefficients of the walls and the target are set to 1.0, which is the ideal case with the maximum echo intensity. The antenna is used for both transmitting and receiving, and is scanned along a straight line. The i-th antenna location is expressed as $x = i\Delta x + x_0$, where Δx is the interval of the antenna location. An antenna is scanned along a line $y = y_0$ in the x direction. Raised-cosine-shaped UWB pulses, with a roll-off factor of 1.0, a center frequency of 79 GHz and a bandwidth of 1.4 GHz, are transmitted and echoes are received by the same antenna. The antenna is assumed to have an ideally uniform beam pattern with a beamwidth of 180° and with the mainlobe in the direction of the y axis. Note that the ideal 180° uniform beam pattern for the entire bandwidth of 1.4 GHz cannot be realized in practice. The purpose of this paper is to evaluate the performance of radar imaging methods in ideal cases, which corresponds to the achievable performance limit. It is an important future task to investigate the imaging quality under actual conditions with a non-uniform antenna pattern, waveform distortion, and antenna coupling effect.

We define $s'(X, Y)$ as the received signal at the antenna location $(x, y) = (X, y_0)$, where we define Y with time t and the speed of the radiowave c as $Y = \mathrm{c}t$. The ray tracing method [14], [15] is used to calculate the received signal. Ray tracing solves the propagation of waves by repeatedly generating narrow beams through the medium. In our simplified model, the waveforms change only their amplitudes and delays, with the signal $s'(Y)$ received at $\boldsymbol{r} = (X, y_0)$ calculated as

$$s'(Y) = \sum_{n=1}^{L} A_n w(Y - \mathrm{c}\tau_n), \tag{1}$$

where L is the number of paths, A_n and τ_n represent the amplitude and relative delay of the n-th component and $w(Y)$ is the reference waveform. The direct echoes from walls are subtracted from $s'(X, Y)$. A filter matched with the transmitted waveform is applied to the raw signal $s'(X, Y)$ to obtain a filtered signal $s(X, Y)$. The imaginary space expressed with (X, Y) is called a data space.

For convenience, we introduce mirror image antennas that are located at symmetrical positions with respect to the room walls as in Fig. 3. Each multipath wave can be modeled with an imaginary echo from the corresponding mirror image antenna. The j-th mirror image antenna for the i-th antenna position is located at $\boldsymbol{a}_i^{(j)} = (x_i^{(j)}, y_i^{(j)}) = (i\Delta x^{(j)} + x_0^{(j)}, y_0^{(j)})$ $(i = 0, \cdots, M;\ j = 0, \cdots, N)$, where M is the number of antenna locations, N is the number of mirror image antennas, and $\Delta x^{(j)}$ is the interval of the j-th mirror image antenna's location. The indexes $j > 0$ are assigned to the mirror image antennas from left to right, and from top to bottom in ascending order. In the case of $j = 0$, it represents an actual antenna location.

3. Conventional Methods

3.1 SEABED Method

A high-speed UWB radar imaging method, SEABED [6] has been proposed based on a simplified target model. This method utilizes a reversible transform BST (Boundary Scattering Transform) between the point of real space (x, y) and the point of data space (X, Y'), which is extracted by the output of the matched filter $s(X, Y)$, where $Y' = Y/2$. The IBST (Inverse BST) is expressed as

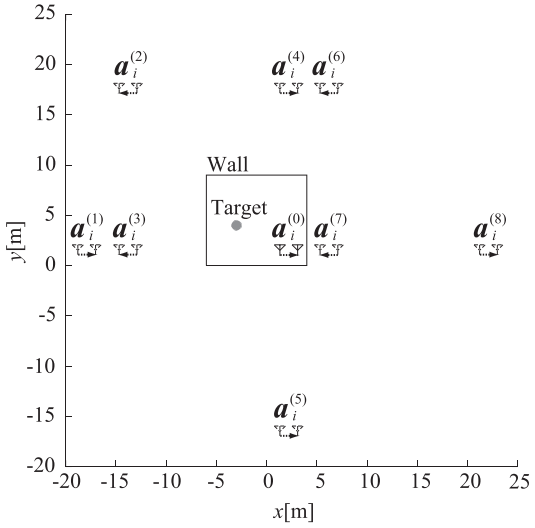

Fig. 4 System model B without shadow regions.

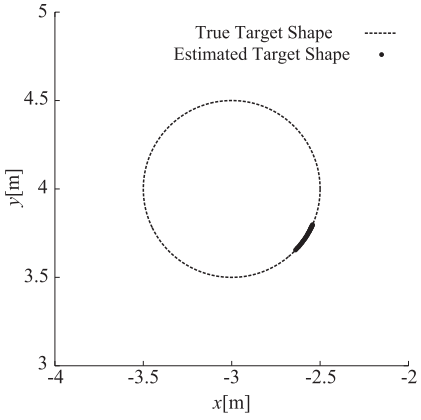

Fig. 5 Image estimated by the SEABED method.

$$\begin{cases} x = X - Y' \, \mathrm{d}Y'/\mathrm{d}X, & (2) \\ y = Y' \sqrt{1 - (\mathrm{d}Y'/\mathrm{d}X)^2}, & (3) \end{cases}$$

where $|\mathrm{d}Y'/\mathrm{d}X| \leq 1$ holds. Although it is reported that the SEABED can obtain a high-quality image, this method can be applied only to measurements using only direct echoes received without any multipath signals as in Fig. 4.

Figure 5 shows the estimated image by applying the IBST to the system model shown in Fig. 4. Here, a circular target with a radius of 0.5 m located at $(-3.0\,\mathrm{m}, 4.0\,\mathrm{m})$ is assumed. We also set the other parameters $(x_0, y_0) = (0.1\,\mathrm{m}, 1.0\,\mathrm{m})$, $\Delta x = 0.1$ m, and $M = 38$. In Fig. 5, although SEABED provides an accurate target shape, we can obtain only a small part of the target shape because we use only direct echoes from the target without any multipath echoes.

3.2 Time-Reversal Imaging Method

The TR (Time-Reversal) method is another approach for UWB radar imaging that is likely to be applicable even to multipath echoes [12]. In the TR method, extended to shadow region imaging, the image $I(\boldsymbol{r})$ is formulated as

$$I(\boldsymbol{r}) = \sum_i \sum_{p=0}^{N} \sum_{q=0}^{N} H(p, q, \boldsymbol{r}) \left| s' \left(X, \left| \boldsymbol{r} - \boldsymbol{a}_i^{(p)} \right| + \left| \boldsymbol{r} - \boldsymbol{a}_i^{(q)} \right| \right) \right|^2, \quad (4)$$

where $H(p, q, \boldsymbol{r})$ is the function defined as

$$H(p, q, \boldsymbol{r}) = \begin{cases} 1 & (\boldsymbol{r} \notin \boldsymbol{\Pi}_p \cup \boldsymbol{\Pi}_q), \\ 0 & (\boldsymbol{r} \in \boldsymbol{\Pi}_p \cup \boldsymbol{\Pi}_q). \end{cases} \quad (5)$$

In Eq. (5), $\boldsymbol{\Pi}_p$ is the shadow region from the location of p-th antenna. Equation (4) indicates that the image $I(\boldsymbol{r})$ is produced by summing all the signals using different antenna pairs after compensating for the time delay. The function $H(p, q, \boldsymbol{r})$ prevents the summation from including contradictory components that propagate through the PEC walls.

We apply this method to the system model shown in Fig. 3. Here, the observation time is $0 \leq t \leq 150$ nsec, corresponding to a range of 45 m. We assume $N = 6$, which means that the image is produced with multipath echoes with the number of reflections equal to or less than 3.

Figure 6 shows the received signals $s(X, Y)$ and Fig. 7 shows the image obtained by the TR method. The image is

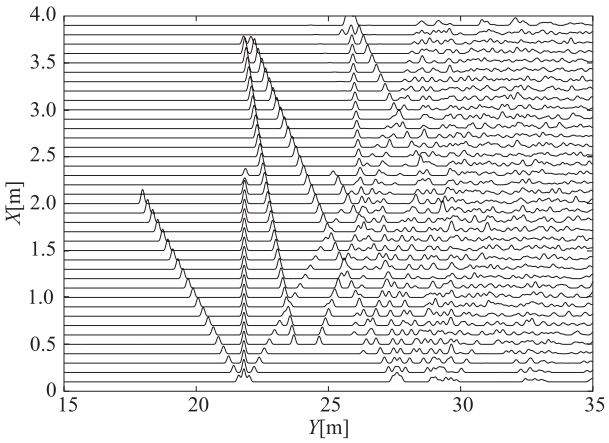

Fig. 6 Received signals after applying the matched filter.

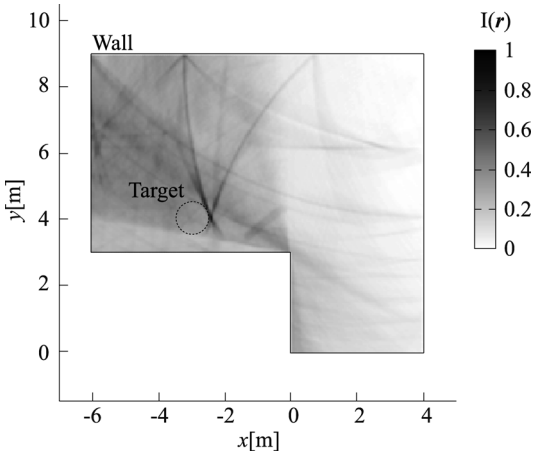

Fig. 7 Image estimated by the TR method.

normalized by the maximum value of $I(\boldsymbol{r})$. As shown in this figure, although the TR method can estimate the location of the target, it cannot estimate an accurate shape thereof.

4. Proposed Method

4.1 Extraction of Range Point Pairs

This section describes the proposed imaging algorithm to obtain high-resolution images in an indoor environment. First, in this subsection, we explain the procedure of the initial data processing of the received signals. $(X_i, Y_{i,k})$ is defined as the range point that is extracted from the peak points of $s(X, Y)$ as

$$\left.\frac{\delta\, s(X,Y)}{\delta\, Y}\right|_{(X,Y)=(X_i,Y_{i,k})} = 0, \tag{6}$$

$$s(X_i, Y_{i,k}) \geq \rho \max s(X, Y), \tag{7}$$

where X_i is the i-th actual location of an antenna and $Y_{i,k}$ is the k-th peak of the signal received at (X_i, y_0). The parameter $\rho \geq 0$ is empirically determined. The k-th peak point for X_i is extracted by finding the local maximum points with the quasi-Newton method as

$$Y_{i,k} = \arg\max_{Y} |s(X_i, Y)|^2, \tag{8}$$

with the initial value $Y = m\Delta Y_\mathrm{s}$ satisfying

$$|s(X_i, (m-1)\Delta Y_\mathrm{s}| < |s(X_i, m\Delta Y_\mathrm{s})| > |s(X_i, (m+1)\Delta Y_\mathrm{s})|. \tag{9}$$

ΔY_s is the sampling interval of Y. The sampled data of the signal $s(X, Y)$ is interpolated using the sinc function in this search. Moreover, we pick up pairs of adjacent range points satisfying the condition:

$$|Y_{i,u} - Y_{i+1,v}| \leq T_0, \tag{10}$$

where T_0 is the length of the transmitted pulse. The schematic of this procedure is illustrated in Fig. 8. We set $T_0 = 0.2\,\mathrm{m}$ for our system with the bandwidth of $B_\mathrm{w} = 1.4\,\mathrm{GHz}$. T_0 is calculated as $T_0 = \mathrm{c}/B_\mathrm{w}$. The black dots connected with solid lines in Fig. 9 show the pairs of range points extracted by the procedure described above.

4.2 Interferometry Imaging in an Indoor Environment

In this subsection, we describe the proposed imaging method using the range points extracted in the previous subsection. Note that the received echoes include both monostatic and bistatic radar echoes. If the transmitting and receiving propagation paths are identical as in the left-hand side figure of Fig. 10, this is interpreted as a monostatic radar signal with a single actual/imaginary antenna. In contrast, other reflected echoes propagate along a path different from the transmitting propagation; this echo corresponds to a bistatic radar arrangement as in the right-hand side figure of Fig. 10.

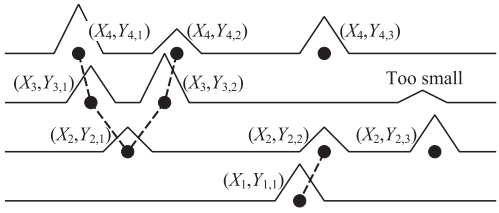

Fig. 8 Schematic of extracting pairs of range points.

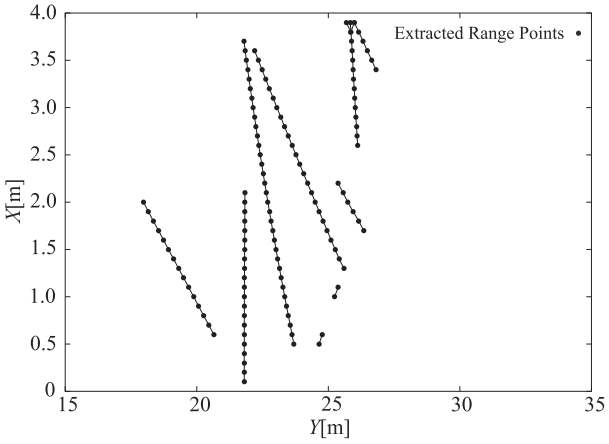

Fig. 9 Extracted pairs of range points.

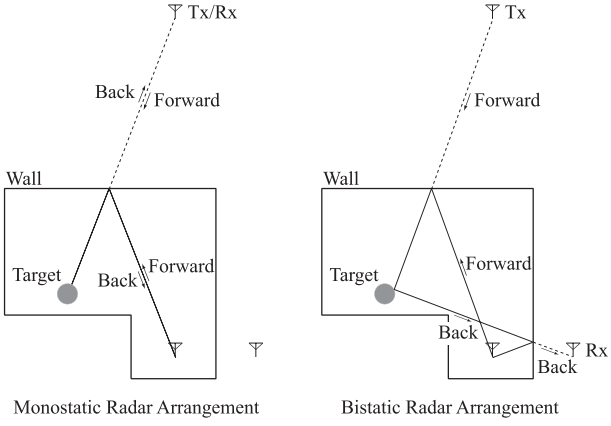

Fig. 10 Two kinds of propagation paths.

The interferometry method [13] is employed for imaging using the extracted pairs of range points. Interferometry is a commonly used technique for DOA (Direction-Of-Arrival) estimation using the phase difference between multiple echoes received with different antennas. By extending this principle, the target shape is provided by solving the intersection points of the following couple of ellipses:

$$\left\{ \left|\boldsymbol{r} - \boldsymbol{a}_i^{(p)}\right| + \left|\boldsymbol{r} - \boldsymbol{a}_i^{(q)}\right| = Y_{i,u}, \right. \tag{11}$$

$$\left. \left|\boldsymbol{r} - \boldsymbol{a}_{i+1}^{(p)}\right| + \left|\boldsymbol{r} - \boldsymbol{a}_{i+1}^{(q)}\right| = Y_{i+1,v}. \right. \tag{12}$$

This can be used for estimating the DOA by measuring the difference between the delays of multiple echoes received by different antennas. The schematic of this interferometry

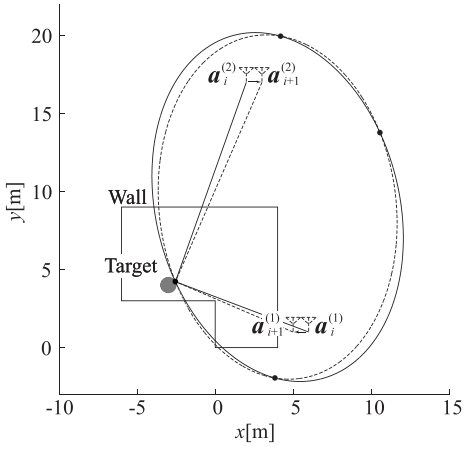

Fig. 11 Schematic of bistatic interferometry.

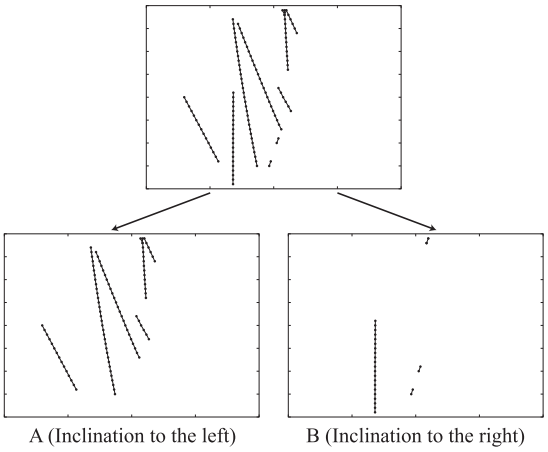

Fig. 13 Schematic of false image reduction process.

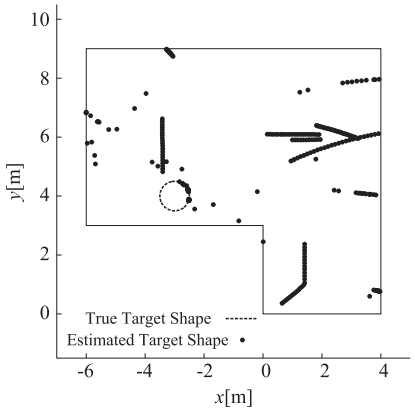

Fig. 12 Estimated image points without false image reduction process.

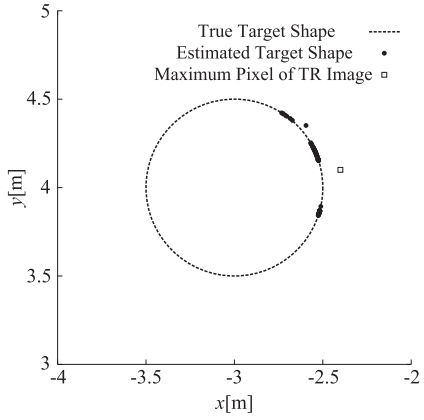

Fig. 14 Estimated image points with false image reduction process.

method is illustrated in Fig. 11, where an ellipse with foci $\boldsymbol{a}_i^{(1)}$ and $\boldsymbol{a}_i^{(2)}$, and another ellipse with foci $\boldsymbol{a}_{i+1}^{(1)}$ and $\boldsymbol{a}_{i+1}^{(2)}$ are used to calculate the target location. In the case of $p = q$, the solution is given by the intersection of a couple of circles, not ellipses. The actual numerical procedure of calculating the intersections of circles or ellipses are explained in Appendices A and B. We apply these methods to all possible combinations of pairs of range points and antennas to obtain an estimated image. Finally, if the estimated point falls outside the room, the point is removed.

The image estimated by this method is shown in Fig. 12, where a broken line and black dots represent the actual target shape and the estimated image. Although this image is a correct estimate of the circular target, it also has many false image points because it contains incorrect combinations of a range of points and antennas. This is because incorrect pairs of antennas are used to produce the image.

4.3 False Image Reduction Method

The problem is that we cannot know which echo corresponds to which antenna pairs at this stage. First, we calculate a rough image using the conventional TR method to estimate the approximate location of targets as in Fig. 7. We estimate the maximum point $\boldsymbol{r}_{\max}$ from the image in Fig. 7. Next, we pick up consistent combinations of range points that satisfy the relationship between the actual/imaginary antenna scanning direction and the estimated range values. We only use antenna pairs based on the inclination of the lines connecting the range points. In this process, echoes are divided into two groups A and B as in Fig. 13. Each antenna pair is classified as a member of one of these groups A or B. Applying the interferometry method, we add the following condition:

$$\begin{cases} Y_{i,u} \geq Y_{i+1,v} & \left(\left|\boldsymbol{r}_{\max} - \boldsymbol{a}_i^{(p)}\right| + \left|\boldsymbol{r}_{\max} - \boldsymbol{a}_i^{(q)}\right| \right. \\ & \left. \geq \left|\boldsymbol{r}_{\max} - \boldsymbol{a}_{i+1}^{(p)}\right| + \left|\boldsymbol{r}_{\max} - \boldsymbol{a}_{i+1}^{(q)}\right|\right), \quad (13) \\ Y_{i,u} < Y_{i+1,v} & \left(\left|\boldsymbol{r}_{\max} - \boldsymbol{a}_i^{(p)}\right| + \left|\boldsymbol{r}_{\max} - \boldsymbol{a}_i^{(q)}\right| \right. \\ & \left. < \left|\boldsymbol{r}_{\max} - \boldsymbol{a}_{i+1}^{(p)}\right| + \left|\boldsymbol{r}_{\max} - \boldsymbol{a}_{i+1}^{(q)}\right|\right). \quad (14) \end{cases}$$

Additionally, we assume that true image points exist within the vicinity of the point $\boldsymbol{r}_{\max}$ as $|\boldsymbol{r} - \boldsymbol{r}_{\max}| < \mu$. The target shape estimated by the proposed method is shown in Fig. 14, where the white square symbol represents the estimated target location $\boldsymbol{r}_{\max}$, and where we set $\mu = 0.5\,\mathrm{m}$

and $\boldsymbol{r}_{\max} = (-2.40\,\mathrm{m}, 4.10\,\mathrm{m})$. In this figure, most of the false images are removed and the true target shape is accurately estimated. The RMS error of the estimated shape is 0.47 mm.

In our numerical simulations, we assume a vacant room without any furniture. However, the proposed method can still be applied even if there are some items of furniture in the room. This is because the method can produce images if it can employ the imaginary mirror antennas corresponding to the propagation paths including the effect of furniture. As for the applicability of the proposed method to a moving target, the performance depends on the scanning speed of the antenna. If the antenna scanning is much faster than the target motion, the proposed method can produce snap-shot images. If an antenna array is employed instead of mechanical scanning, the method can easily be applied to a moving target.

4.4 Parameter Optimization

The parameters ρ and μ in our proposed algorithm have a significant effect on imaging performance. In this subsection, we investigate the estimated range and accuracy of images for varying values of parameters ρ and μ. Figure 15 and Fig. 16 show the estimated range and the estimation RMS error for the parameter ρ and μ, where the estimated range is the percentage of the estimated area of the target surface over the total surface area. The results reveal that there is a trade-off relationship between the estimated range and accuracy. To ensure an estimated range of more than 7%, the parameter pair (ρ, μ) needs to be set to $(0.3, 0.4)$, $(0.4, 0.5)$ or $(0.5, 0.5)$ as shown in Fig. 15. Moreover, to obtain the minimum RMS error under the previous condition, the parameter pair (ρ, μ) is set to $(0.5, 0.5)$ as shown in Fig. 16. Hereafter, we use these values for our numerical simulations. Note that we assume the system model A in calculating these values. However, the optimum parameters depend on the target size, shape and location, as well as the room shape.

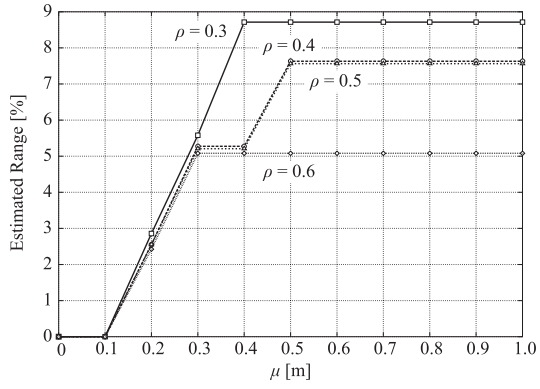

Fig. 15 Estimated range for the parameters ρ and μ.

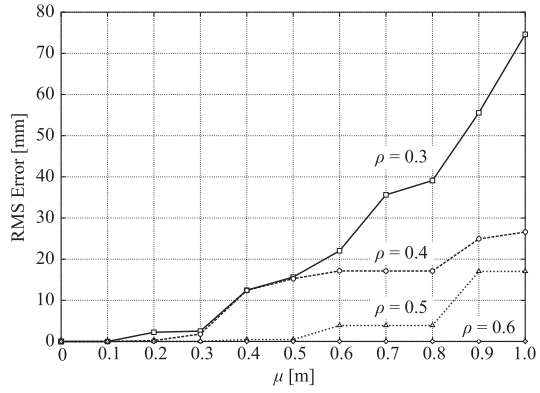

Fig. 16 RMS error for the parameters ρ and μ.

5. Performance Evaluation of the Proposed Method

5.1 Noise Tolerance

We show the imaging accuracy of the proposed method with noisy data assuming the same scenario as in the previous section. To produce a noisy signal numerically, white Gaussian noise is added to the raw signals $s'(X, Y)$. We define S/N as the ratio of the peak instantaneous signal power to the averaged noise power after applying the matched filter. The RMS error of the estimated shape using the proposed method is shown in Fig. 17. This figure shows that the RMS error is relatively small, less than 40 mm for the S/N $\geq$ 26.50 dB. Moreover, we have confirmed that the TR method cannot estimate an accurate target location in the case of S/N $\leq$ 15.73 dB, leading to poor performance of the proposed method. The image estimated in noisy environments is shown in Fig. 18 for S/N = 30.50 dB. In Fig. 18, although there are inappropriate false points, most of the estimated points are located on the target surface, giving an accurate image estimation.

5.2 Performance Evaluation with Other Models

This subsection discusses the performance of the proposed method with different models. First, we apply the proposed method to the system model B shown in Fig. 4. The target image obtained is shown in Fig. 19. This result verifies

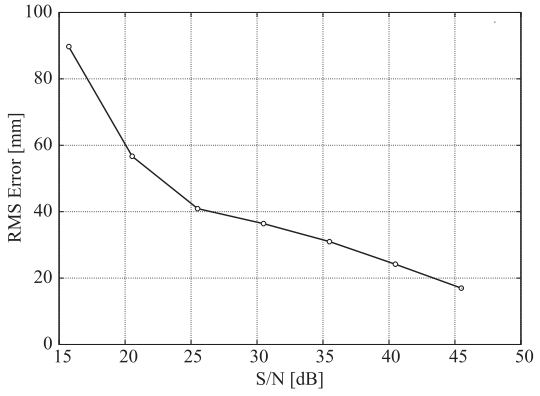

Fig. 17 RMS error of the proposed method vs. S/N.

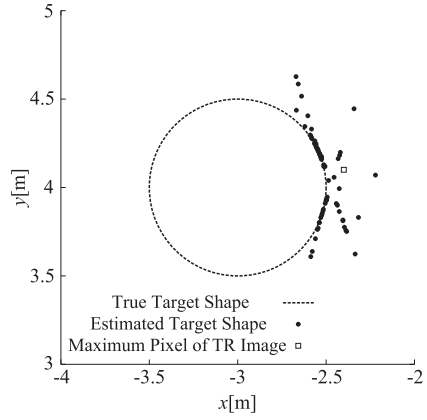

Fig. 18 Estimated image points for S/N=30.50 dB.

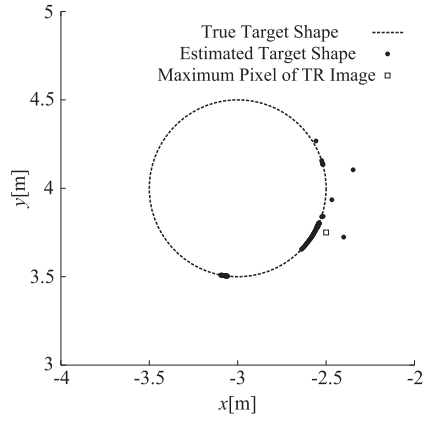

Fig. 19 Estimated image points for a target in a line-of-sight area.

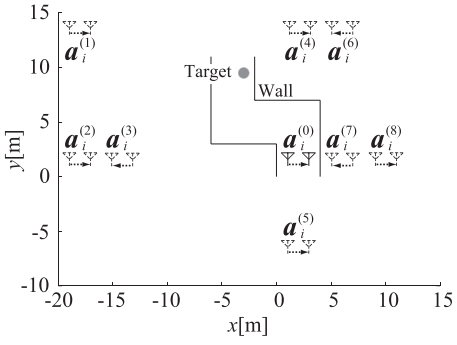

Fig. 20 System model C for a hallway.

that the region containing images is extended compared with Fig. 5 because the proposed method uses not only the direct echo but also multipath echoes for imaging. The estimation RMS error is 1.78 mm.

Next, we show the performance of the proposed method assuming the environment shown in Fig. 20, modeling a corner of a hallway. The estimated image is shown in Fig. 21. In this figure, a different part of the target boundary is accurately estimated. The estimation RMS error is 33.19 mm.

Finally, we apply the proposed method to an elliptical PEC target in the model A shown in Fig. 3. Figure 22 shows an example of the estimated image for the target with an inclination angle of 120°, where part of the target shape is correctly estimated with an estimation RMS error of 0.02 mm. We have also applied the proposed method to the same elliptical targets with various inclination angles for $60° \leq \psi \leq 120°$ and confirmed the average estimation RMS error to be 2.57 mm.

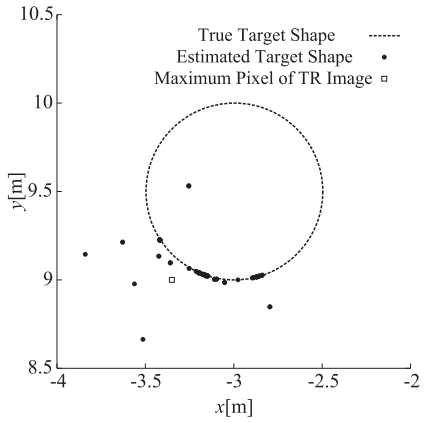

Fig. 21 Image estimated for the system model C.

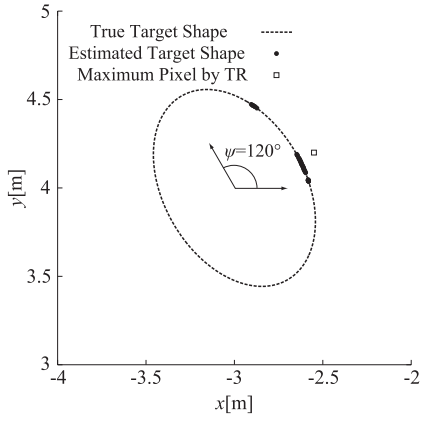

Fig. 22 Estimated image points for an elliptical target.

The accuracy of estimation depends on many factors including the target shape and location, and the room shape. This is because the interference effect between echoes from different paths is highly sensitive to these factors. In addition, the optimum parameters ρ and μ depend on assumptions of the room's shape, the wall's reflectivity and the target location. As such, it is difficult to evaluate the imaging accuracy in a general context.

6. Conclusions

This paper proposed a single antenna imaging method for targets in shadow regions. First, we established that the conventional method does not provide sufficient resolution of a target in a shadow region. To obtain a high-resolution image, we proposed the imaging method using the princi-

ple of interferometry and applied this method to each of the mirror image antennas. Additionally, we proposed a false image reduction algorithm using an approximate target location obtained by the TR method and the inclination of the estimated pairs of echoes in the data space. In this process, most of the false image points were removed and the target boundary was estimated accurately. We also investigated the performance of the proposed method for noisy data and clarified that an accurate image is obtained when the S/N is higher than about 25 dB based on the results of the computer simulations. Moreover, we investigated the performance of the proposed method in different system models, confirming the effectiveness of the proposed method in a variety of situations. Note that the performance of the proposed method evaluated in the paper is based on a few particular models. Therefore, the performance depends on multiple factors including the reflection coefficients of the walls and target, and the parameters ρ and μ. The proposed method assumes a system model with a single target, and the algorithm is assumed to know this model. To apply the method to multiple targets, it is expected that some modifications would be required to the method. For example, the peak detection process of the TR method needs to be adequately modified to extract multiple peaks. This expansion of the method to multiple targets is an important future task.

References

[1] S. Ikeda, H. Tsuji, and T. Ohtsuki, "Indoor event detection with eigenvector spanning signal subspace for home or office security," IEICE Trans. Commun., vol.E92-B, no.7, pp.2406–2412, July 2009.
[2] K. Pahlavan, F.O. Akgul, M. Heidari, A. Hatami, J.M. Elwell, and R.D. Tingley, "Indoor geolocation in the absence of direct path," IEEE Wireless Commun., vol.13, no.6, pp.50–58, 2006.
[3] C. Le, T. Dogaru, L. Nguyen, and M.R. Ressler, "Ultra wideband (UWB) radar imaging of building interior: Measurements and predictions," IEEE Trans. Geosci. Remote Sens., vol.47, no.5, pp.1409–1420, 2009.
[4] X. Zhuge, T.G. Savelyev, A.G. Yarovoy, and L.P. Ligthart, "UWB array-based radar imaging using modified Kirchhoff migration," 2008 IEEE International Conference on Ultra-WideBand (ICUWB2008), vol.3, pp.175–178, 2008
[5] W.C. Khor, M.E. Bialkowski, A. Abbosh, N. Seman, and S. Crozier, "An ultra wideband microwave imaging system for breast cancer detection," IEICE Trans. Commun., vol.E90-B, no.9, pp.2376–2380, Sept. 2007.
[6] T. Sakamoto, "A fast algorithm for 3-D imaging with UWB pulse radar systems," IEICE Trans. Commun., vol.E90-B, no.3, pp.636–644, March 2007.
[7] S. Kidera, Y. Kani, T. Sakamoto, and T. Sato, "A fast and high-resolution 3-D imaging algorithm with linear array antennas for UWB pulse radars," IEICE Trans. Commun., vol.E91-B, no.8, pp.2683–2691, Aug. 2008
[8] T. Sakamoto, Y. Matsuki, and T. Sato, "A novel UWB radar 2-D imaging method with a small number of antennas for targets with arbitrary shapes and motion," 2009 IEEE International Conference on Ultra-WideBand (ICUWB2009), pp.9–11, 2009.
[9] E.A. Marengo and F.K. Gruber, "Subspace-based localization and inverse scattering of multiple scattering point targets," EURASIP J. Appl. Signal Process., vol.2007, pp.192–192, 2007.
[10] Y. Jin and J.M.E. Moura, "Time-reversal detection using antenna arrays," IEEE Trans. Signal Process., vol.57, pp.1396–1414, 2009.
[11] T. Sakamoto and T. Sato, "Time-reversal UWB imaging with a single antenna in multi-path environments," 3rd European Conference on Antennas and Propagation (EuCAP) 2009, pp.23–37, 2009.
[12] T. Sakamoto and T. Sato, "A method of estimating a room shape with a single antenna in a multipath environment," 4th European Conference on Antennas and Propagation (EuCAP) 2010, pp.12–16, 2010.
[13] D. Massonet and K.L. Feigl, "Radar interferometry and its applications to changes in Earth's surface," Rev. Geophys., vol.36, no.4, pp.441–500, 1998.
[14] M.F. Iskander and Z. Yun, "Propagation prediction models for wireless communication systems," IEEE Trans. Microw. Theory Tech., vol.50, pp.662–673, 2002.
[15] M.C. Lawton and J.P. McGeehan, "The application of a deterministic ray launching algorithm for the prediction of radio channel characteristics in small-cell environments," IEEE Trans. Veh. Technol., vol.43, pp.955–968, 1994.

Appendix A: Monostatic Interferometry Method

The intersection point of two circles Eqs. (11) and (12) for $p = q$ is analytically solved by

$$\boldsymbol{r} = \boldsymbol{a}_i^{(p)} + Y_{i,m} \begin{pmatrix} \cos(\alpha \pm \beta) \\ \sin(\alpha \pm \beta) \end{pmatrix}, \tag{A·1}$$

where α and β are represented as

$$\alpha = \tan^{-1}\left(\frac{y_i^{(p)} - y_{i+1}^{(p)}}{x_i^{(p)} - x_{i+1}^{(p)}}\right), \tag{A·2}$$

$$\beta = \cos^{-1}\left(\frac{(x_i^{(p)} - x_{i+1}^{(p)})^2 + (y_i^{(p)} - y_{i+1}^{(p)})^2 + Y_{i,m}^2 - Y_{i+1,n}^2}{2Y_{i,m}\sqrt{(x_i^{(p)} - x_{i+1}^{(p)})^2 + (y_i^{(p)} - y_{i+1}^{(p)})^2}}\right). \tag{A·3}$$

Appendix B: Bistatic Interferometry Method

The intersection point of two ellipses is solved numerically. The ellipse defined by Eq. (11) is expressed with the parameter θ in the following equation:

$$\boldsymbol{r}(\theta) = \boldsymbol{R}(\gamma) \begin{pmatrix} a\cos\theta \\ b\sin\theta \end{pmatrix} + \frac{\boldsymbol{a}_i^{(p)} + \boldsymbol{a}_i^{(q)}}{2} \quad (0 \le \theta \le 2\pi), \tag{A·4}$$

where $\boldsymbol{R}(\cdot)$ represents the rotation matrix:

$$\boldsymbol{R}(\phi) = \begin{pmatrix} \cos\phi & -\sin\phi \\ \sin\phi & \cos\phi \end{pmatrix}, \tag{A·5}$$

and γ is a constant number given by

$$\gamma = \tan^{-1}\left(\frac{y_i^{(p)} - y_i^{(q)}}{x_i^{(p)} - x_i^{(q)}}\right). \tag{A·6}$$

The parameters a and b denote the long and short axes of the ellipse in Eq. (11), given by

$$a = Y_{i,m}/2, \tag{A·7}$$

$$b = \sqrt{Y_{i,m}^2 - (x_i^{(p)} - x_i^{(q)})^2 - (y_i^{(p)} - y_i^{(q)})^2} \Big/ 2. \qquad (\mathrm{A}\cdot 8)$$

When the point $\boldsymbol{r}(\theta)$ corresponds to the intersection point, the point satisfies Eq. (12). To use this principle for calculation, the following function $F(\theta)$ is introduced:

$$F(\theta) = \left|\boldsymbol{r}(\theta) - \boldsymbol{a}_{i+1}^{(p)}\right| + \left|\boldsymbol{r}(\theta) - \boldsymbol{a}_{i+1}^{(q)}\right| - Y_{i+1,n}. \qquad (\mathrm{A}\cdot 9)$$

We find θ^* by numerical calculation, where the θ^* satisfies $F(\theta^*) = 0$. The solution is given as $\boldsymbol{r}(\theta^*)$.

Shuhei Fujita received the B.E. degree from Kyoto University in 2010. He is currently studying for an M.I. degree at the Graduate School of Informatics, Kyoto University. His current research interest is in signal processing for UWB pulse radars.

Takuya Sakamoto received his B.E. degree from Kyoto University in 2000, and M.I. and Ph.D. degrees from the Graduate School of Informatics, Kyoto University in 2002 and 2005. He is an assistant professor in the Department of Communications and Computer Engineering, Graduate School of Informatics, Kyoto University. His current research interest is in UWB radar signal processing. He is a member of the IEEJ and the IEEE.

Toru Sato received his B.E., M.E., and Ph.D. degrees in Electrical Engineering from Kyoto University, Kyoto, Japan in 1976, 1978, and 1982. He has been with Kyoto University since 1983 and is currently a Professor in the Department of Communications and Computer Engineering, Graduate School of Informatics. His major research interests include system design and signal processing aspects of UWB radars, atmospheric radars, radar remote sensing of the atmosphere, and radar observation of space debris. He is a member of the Institute of Electrical and Electronics Engineers, the Society of Geomagnetism and Earth, Planetary and Space Sciences, the Japan Society for Aeronautical and Space Sciences, and American Meteorological Society.